Bulletin of Earthquake Engineering (2019) 17:473–495
https://doi.org/10.1007/s10518-018-0452-3

ORIGINAL RESEARCH

Diaphragm effectiveness of precast concrete structures with cladding panels under seismic action

Bruno Dal Lago[1] · **Silvia Bianchi**[1] · **Fabio Biondini**[1]

Received: 28 November 2017 / Accepted: 11 August 2018 / Published online: 27 August 2018

Abstract
The seismic performance of precast frame structures strongly depends on the mechanical devices connecting both structural and non-structural elements. Following recent post-earthquake field observations of unintended seismic interaction of the cladding panels with the frame structure, the seismic design of the cladded system is currently being critically examined by the scientific community. Design solutions involving a controlled cladding–structure interaction have been proposed to address this problem. However, the frame–panel interaction may draw high stresses into the roof diaphragm, as a consequence of the stiffening of the external frames only. This paper presents a parametric study based on linear and non-linear dynamic analyses investigating different levels of interaction among frames, panels, and diaphragm system. The results show how the deck and cladding connections influence the seismic behaviour of the structure. Innovative fastening systems aimed at enhancing the seismic performance of the structure are proposed based on the use of dissipative connection devices inserted into both cladding and deck components.

Keywords Precast structures · Mechanical connections · Dissipative devices · Diaphragm action · Seismic performance · Non-linear analysis

1 Introduction

The seismic behaviour of dry-assembled precast frame structures has been thoroughly investigated in the last two decades, identifying those technological issues which deserve special detailing to achieve satisfactory seismic performance. The value of the behaviour factor to be used in a force-based design of precast concrete frames has been validated in Biondini and Toniolo (2009) on the basis of probabilistic analyses and experimental tests. Capacity design criteria for multi-storey precast frames have been proposed in Biondini et al. (2010). More recently, alternative displacement-based design procedures have been developed in Belleri (2017) and Dal Lago and Molina (2018). The large deformability and ductility capacities of precast structures having correct connection and member details

✉ Bruno Dal Lago
brunoalberto.dallago@polimi.it

[1] Department of Civil and Environmental Engineering, Politecnico di Milano, Piazza Leonardo da Vinci 32, 20133 Milan, Italy

have been confirmed by the results of several experimental tests conducted on full-scale structural prototypes (Priestley et al. 1999; Fischinger et al. 2008; Biondini and Toniolo 2009; Biondini et al. 2012; Negro et al. 2013; Brunesi et al. 2015; Dal Lago et al. 2017a, c, 2018d; Negro and Lamperti Tornaghi 2017; Toniolo and Dal Lago 2017). The structural behaviour of the main mechanical connections has been also studied by means of tests on individual devices or structural sub-assemblies. Column-foundation mechanical connections have been tested by Saisi and Toniolo (1999), Metelli et al. (2011a), Dal Lago et al. (2016), Orlando and Piscitelli (2018), and Tullini and Minghini (2016). Beam-column connections have been tested by Vintzeleou and Tassios (1987), Tsoukantas and Tassios (1989), Dei Poli et al. (1992), Psycharis and Mouzakis (2012a, b), Magliulo et al. (2015), Zoubek et al. (2015), Yuksel et al. (2015), and Muciaccia et al. (2017). Roof-to-beam connections have been tested by Belleri et al. (2014) and Dal Lago et al. (2017d). Panel connections have been tested by Metelli et al. (2011b), Belleri et al. (2016), Zoubek et al. (2016, 2018), Dal Lago et al. (2017a, b, 2018a, b), Yuksel et al. (2017), Dal Lago and Lamperti Tornaghi (2018), and Psycharis et al. (2018).

The field observations after recent earthquakes reported by Toniolo and Colombo (2012), Bournas et al. (2013b), Magliulo et al. (2014b), Belleri et al. (2015a), and Savoia et al. (2017) underline the problem of displacement compatibility between precast frames and cladding panels, whose seismic interaction has been investigated by Biondini et al. (2013a), Magliulo et al. (2014a), Scotta et al. (2015) and Belleri et al. (2018). Retrofit solutions have been proposed by Valente (2013), Belleri et al. (2015b, 2017), Magliulo et al. (2017), Sorace and Terenzi (2017), Dal Lago et al. (2018a), and Pollini et al. (2018). The seismic fragility of precast structures, addressed in literature by Kramar et al. (2010), Titi and Biondini (2014), Casotto et al. (2015), Belleri et al. (2015b), Babič and Dolšek (2016), Buratti et al. (2017), Demartino et al. (2017), Palanci et al. (2017), Titi et al. (2018), and Ercolino et al. (2018), may be strongly influenced by the connection system of the cladding panels. Moreover, a cladding connection system which involves in-plane interaction of the panels with the structure leads to highly non-uniform distribution of stiffness among the various frames of the buildings, acting in parallel, with the external cladded frames being much stiffer than the internal frames. In this way, the horizontal actions tend to redistribute towards the cladding panels, loading the diaphragm with higher stresses.

The diaphragm behaviour of precast roofing systems with structural concrete topping has been addressed in literature by Fleischman and Farrow (2001, 2003) and Fleischman et al. (2005a, b), among others. The diaphragm behaviour of dry-assembled precast decks, which cannot rely on a structural topping to stiffen the diaphragm, has been investigated by Ferrara and Toniolo (2008), Biondini et al. (2013b), Belletti et al. (2015), and Dal Lago and Ferrara (2016) with reference to specific dry-assembled structural arrangements. Experimental results on the diaphragm behaviour of full-scale dry-assembled precast prototypes subjected to seismic excitation have been reported by Biondini and Toniolo (2009), Schoettler et al. (2009), and Bournas et al. (2013a), showing that also dry-assembled diaphragms can provide relevant stiffness and strength, mainly relying on the mechanical connections of the deck elements.

The present paper investigates the seismic behaviour of precast buildings having various layouts of the diaphragm and of the cladding panel connection system through linear and non-linear dynamic analyses. In particular, three different types of connection are investigated: (1) roof-to-beam, (2) floor-to-floor, and (3) panel-to-panel connections. Different stiffness conditions of the deck are investigated by changing the connection types (1) and (2) from low stiffness with flexible roof-to-beam connections on unconnected floor elements to high stiffness with roof-to-beam conditions on

mutually connected roof elements. Different stiffness distributions are investigated by changing the connections type (3), from uniform distribution without mutual panel-to-panel connections to highly non-uniform distribution with stiff panel-to-panel connections.

The effectiveness of dissipative panel and/or deck connections in improving the seismic behaviour of the overall structure by reducing its drift under controlled forces is also assessed by means of non-linear dynamic analysis.

2 Case study

A precast structure with layout and dimensions typical of Southern European industrial buildings is considered as a case study. It is a single-storey two-bay precast frame, made of three lines of columns spaced by 15 m. The columns are 7 m tall with a square section 0.6×0.6 m. The beams have rectangular section 0.6×0.8 m and span of 10 m. The roof elements are 15 m long and have TT section 0.6 m deep and 2.5 m wide. The distributed mass of structural and non-structural dead load is 320 kg/m^2. The peripheral vertical cladding panels have dimensions 2.50×8.75 m with effective thickness of 0.12 m leading to a mass of 300 kg/m^2. The cladding panels are placed along the two long sides of the building and parallel to the beams. All elements are made of concrete C45/55 ($f_{ck} = 45$ MPa). Figure 1 shows the geometry of the building and the scheme of the connections. Three roof-to-roof connections are located at the quarters of span of the elements. Three panel-to-panel connections are placed at the quarters of the distance between bottom and top hinges of each panel. The internal frame is identified by the alignment B, while the external frames are identified by the alignments A and C.

Figure 2 shows a view of the 3D structural model of the building developed using the code Straus 7 (G + D Computing 2010). Columns and beams are modelled with beam elements. The columns are clamped to the foundation. Each beam end is connected to a column with a couple of dowels aligned in the direction orthogonal to the beam element. This connection is idealised with a hinge in the main bending plane of the beam and a monolithic joint in the other planes. The top of the columns and the centroid of the beams are connected by translational coupling links (Fig. 3). Roof elements and cladding panels are modelled with shell elements. Each roof-to-beam connection is modelled with a translational spring with very high translational stiffness in both the vertical (axis z in Fig. 3a) and horizontal direction orthogonal to roof elements (axis y in Fig. 3a). The stiffness associated with the direction parallel to the roof elements (axis x in Fig. 3a), which is among the investigated connections, is varied through the analyses. The distance between the centroid of the beam and the corner node of the rib plate element is covered by a translational coupling link (Fig. 3). The cladding panels are connected to the foundation beams at the bottom and to the peripheral beams at the top with hinged connections. Thus, the central nodes at the base of the panels are restrained, while the top connection is modelled with a spring with high stiffness restraining the relative displacements between the beam and the panel nodes. The mass is distributed according to the material density of the structural elements (2500 kg/m^3). The additional mass associated with waterproofing and finishes on top of the roof elements is considered negligible.

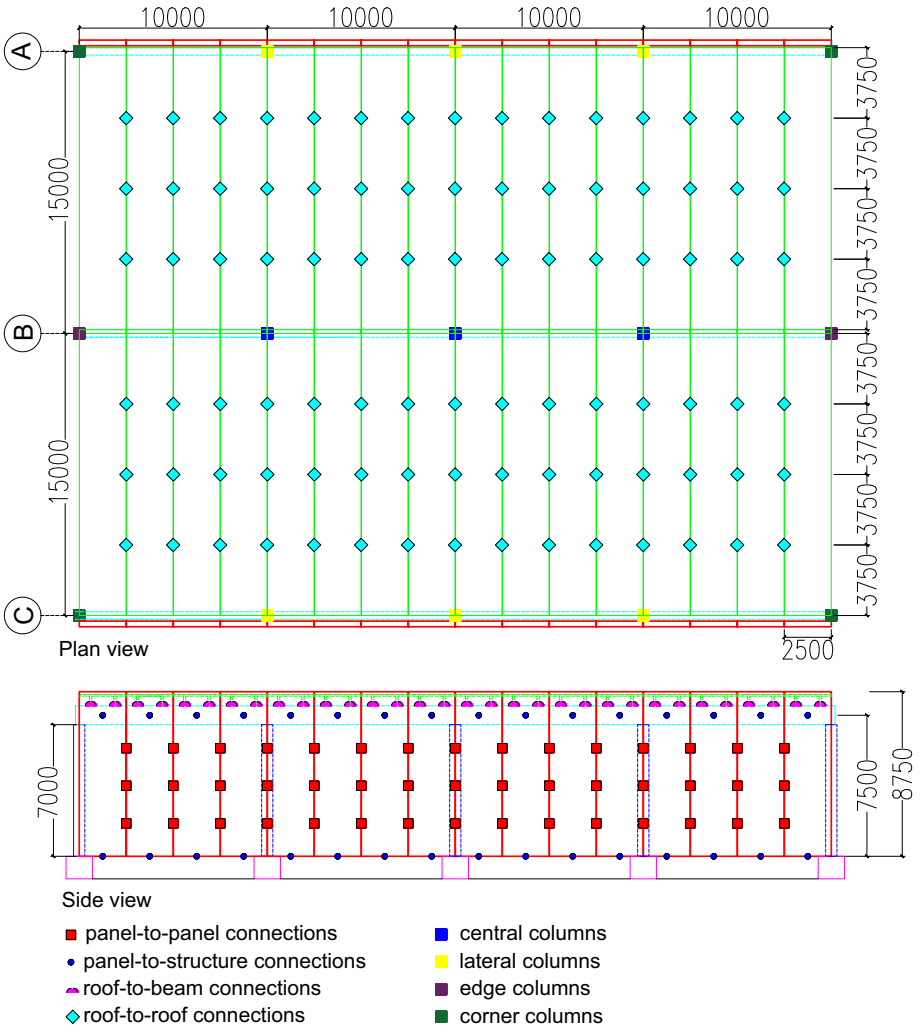

Fig. 1 Case study building (dimensions in mm)

3 Natural frequencies and vibration modes

The natural frequencies and the associated vibration modes of the case study building are investigated by combining different stiffness values of the considered connections. These values have been chosen considering the order of magnitude of the elastic stiffness of mechanical connections tested within the European research projects SAFECAST (Dal Lago et al. 2016, 2017c, d, 2018d) and SAFECLADDING (Biondini et al. 2013a; Dal Lago et al. 2017a, b, 2018a, b, c; Toniolo and Dal Lago 2017). The following values of elastic stiffness are considered for beam-roof connections k_{b-r} (kN/m):

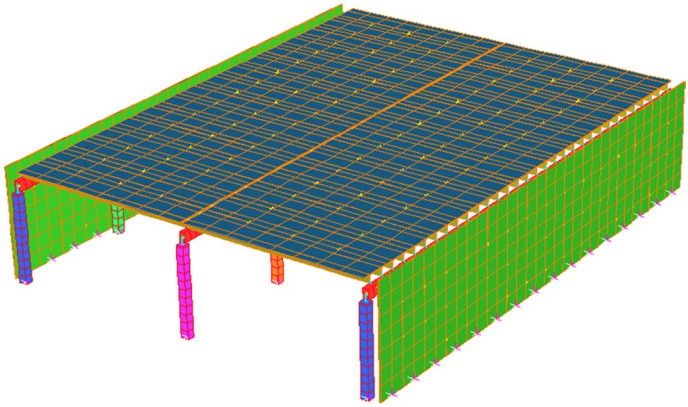

Fig. 2 3D view of the structural model

- $k_{b-r}=10^3$, order of magnitude for elastic stiffness of thin angle connections after activation (see Dal Lago et al. 2017d);
- $k_{b-r}=10^4$, order of magnitude for elastic stiffness of thick angle connections after activation (see Dal Lago et al. 2017d) or for dowel connections with small diameter;
- $k_{b-r}=10^5$, order of magnitude for elastic stiffness for dowel connections with large diameter (see Psycharis and Mouzakis 2012b);
- $k_{b-r}=10^{10}$, order of magnitude for rigid connections, such as welded connections.

The following values are considered for both roof-to-roof connections k_{r-r} and panel-to-panel connections k_{p-p} (kN/m):

- $k_{r-r}=k_{p-p}=0$, no connections;
- $k_{r-r}=k_{p-p}=10^4$, order of magnitude of the elastic stiffness of bolted Multiple Slit Devices (MSDs—see Dal Lago et al. 2018b);
- $k_{r-r}=k_{p-p}=10^5$, order of magnitude of the elastic stiffness of friction-based devices (FBDs—see Dal Lago et al. 2017a);
- $k_{r-r}=k_{p-p}=10^6$, order of magnitude for elastic stiffness of welded rectangular metallic plates (Schultz et al. 1994);
- $k_{r-r}=k_{p-p}=10^{10}$, order of magnitude for rigid connections, such as welded bar connections.

Combining the elastic stiffness of the three orders of connections, $4\times5\times5=100$ analyses have been performed to identify natural frequencies and vibration modes. Following Eurocode 8 (EN 1998-1:2004), half of the cross-sectional elastic stiffness is attributed to the column elements to account for cracking. Figure 4 shows the trends of natural frequencies and corresponding participation factors for different values of roof-to-beams connection stiffness k_{r-b}. The diagrams are shown for increasing values of panel-to-panel stiffness k_{p-p} and for different values of the roof-to-roof stiffness k_{r-r}. Figures 5, 6 and 7 show the deformed shape associated with the main vibration modes of the structure.

The condition $k_{p-p}=0$ is associated with a natural frequency of about 0.96 Hz, regardless the values of k_{r-b} and k_{r-r} (Fig. 4a, c, e, g). In this case, the structure is quite flexible and characterised by a good diaphragm action even with low stiffness of the deck

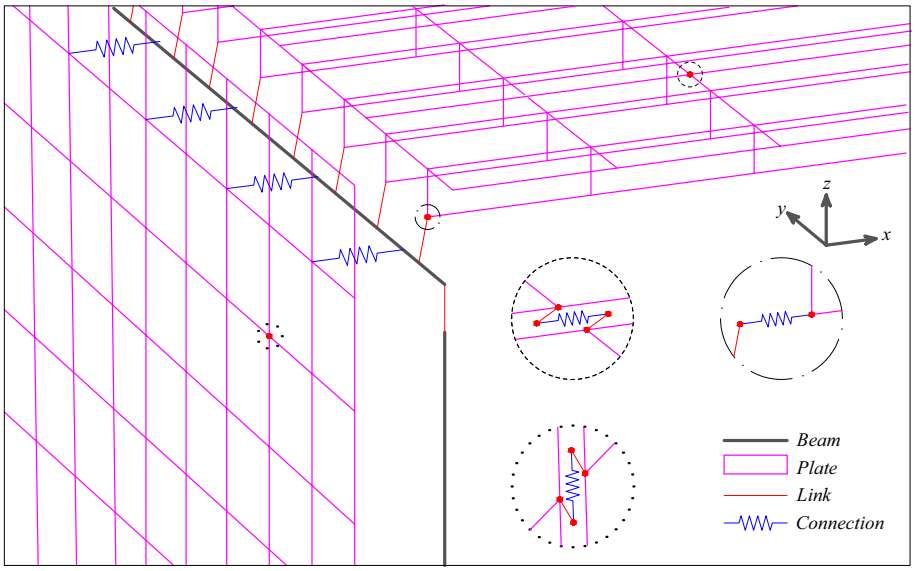

(a)

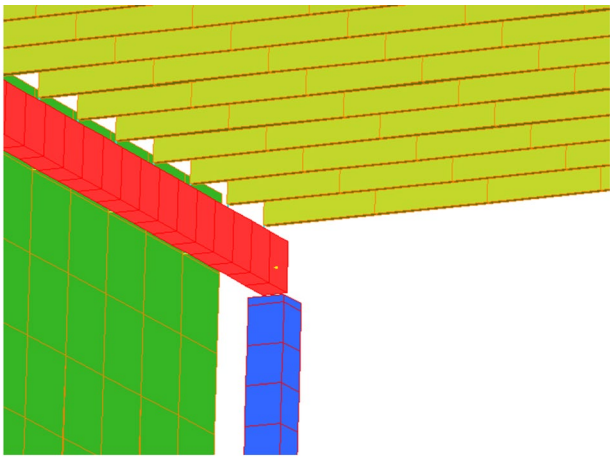

(b)

Fig. 3 Structural model: **a** scheme of elements and connections; **b** 3D solid view

connections. The corresponding vibration mode shows the in-phase displacement of internal and external frames without in-plane distortions (see Fig. 5a). This effect is due to the uniform distribution of mass and stiffness among frames. Moreover, a constant participation factor of about 90% is achieved for the first vibration mode (Fig. 4b, d, f, h).

For increasing values of k_{p-p}, progressive stiffening of external frames occurs. The diaphragm becomes more stressed as the stiffness uniformity among the frames decreases. For low values of k_{r-b} (Fig. 4a), the increase of stiffness for other connections modifies the natural frequency, which grows from 0.96 to 1.8 Hz for values of

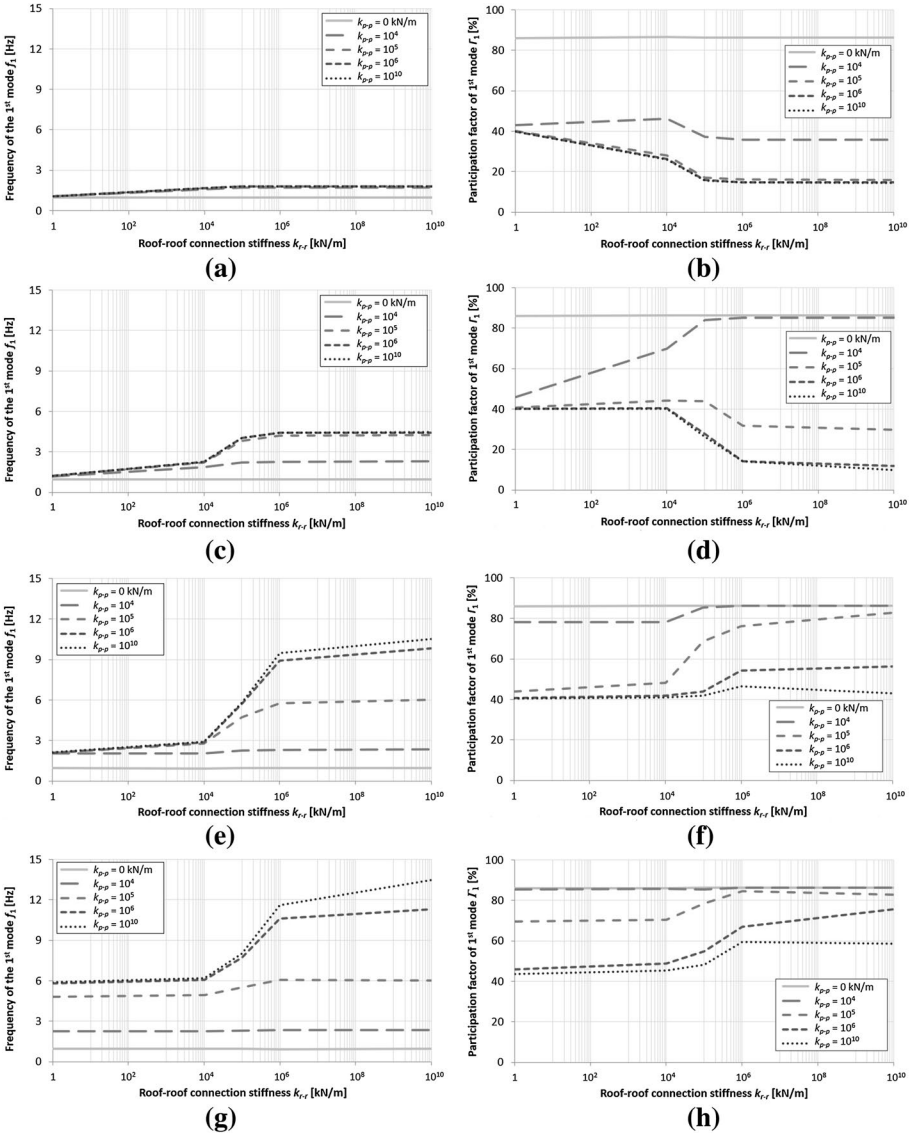

Fig. 4 Natural frequency and participation factor of the first vibration mode of the buildings versus the roof-to-roof connection stiffness k_{r-r} for different values of the panel connection stiffness k_{p-p} = 0, 10^4, 10^5, 10^6, 10^{10} and different values of the roof-to-beam stiffness k_{r-b}: **a**, **b** k_{r-b} = 10^3; **c**, **d** k_{r-b} = 10^4; **e**, **f** k_{r-b} = 10^5; **g**, **h** k_{r-b} = 10^{10} (kN/m)

k_{r-r} up to 10^5 kN/m, remaining constant for higher values. Figure 5b shows that the deformed shape of the building associated with the first vibration mode does not change from the case of no panel-to-panel and roof-to-roof connections to the case of panel-to-panel connections with rigid roof-to-roof connections, indicating a good diaphragm

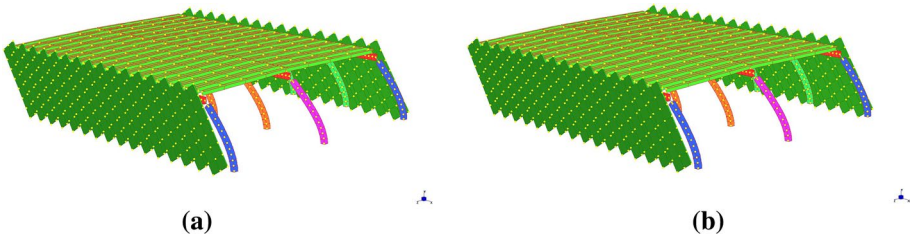

Fig. 5 First vibration mode of the building: **a** $k_{p-p}=0$, $k_{r-r}=0$, $k_{r-b}=10^4$; **b** $k_{p-p}=10^4$, $k_{r-r}=10^5$, $k_{r-b}=10^4$ (kN/m)

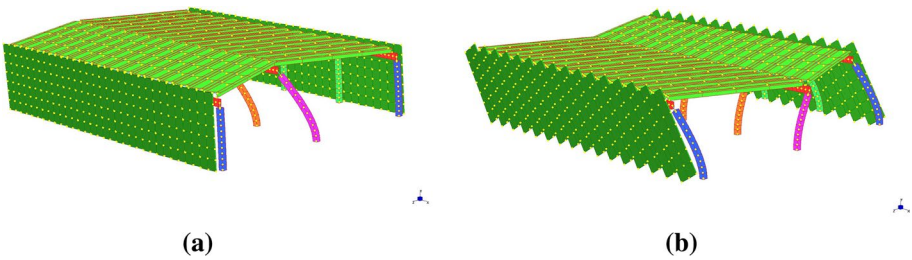

Fig. 6 Building with stiffness of the connections $k_{p-p}=10^4$, $k_{r-r}=0$, and $k_{r-b}=10^4$ (kN/m): **a** first vibration mode; **b** second vibration mode

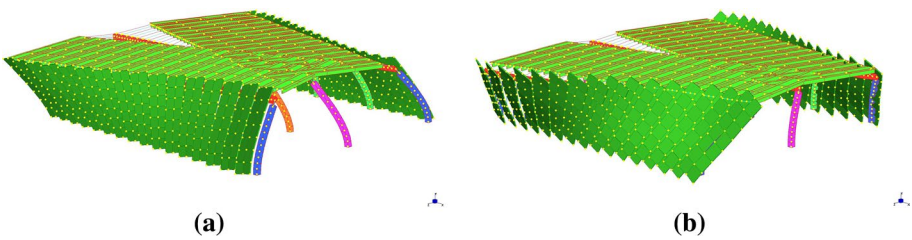

Fig. 7 Building with stiffness of the connections $k_{p-p}=10^4$, $k_{r-r}=10^{10}$, and $k_{r-b}=10^3$ kN/m: **a** first vibration mode; **b** second vibration mode

behaviour. Figure 6 shows the two most significant vibration modes of the structure without roof-to-roof connections, with the first mode associated with the deformation of the central frame, and the second mode related to phase opposition deformations of the external and central frames. In both cases, an important floor distortion occurs.

The diaphragm effect is limited when using flexible roof-to-beam connections, also in case of very stiff roof-to-roof connections. Figure 7 shows the main vibration modes related to this configuration. The deck is subjected to local torsional rotations in each building span and, consequently, an important distortion occurs despite the global base torsional moment is null. The difference between the deformed shapes associated with the two main vibration modes consists in the activation of the relative vertical sliding of the panels. The peculiar deformed configuration depicted in Fig. 7 is not desirable, since the rigid rotation of portions of the deck involves the concentration of displacement

demand in the edge roof-to-beam connections, which could lead to loss of support and out-of-plane relative movements of the panels.

The values of the participation factor of the first natural vibration mode for low k_{r-b} gradually decrease with the increase of k_{p-p}. The participating mass progressively increases for the stiffer vibration modes associated with the external frames, which indicates an inadequate diaphragm action. For higher values of k_{r-b}, the stiffening effect of the external frames is more effectively transmitted to the internal frame, with a dynamic behaviour associated primarily with the first mode. For the stiffer combinations of connections, the frequency associated with the first vibration mode attains a maximum value of 13.8 Hz (Fig. 4g).

For increasing values of k_{r-b} and k_{r-r}, a gradual increase of the participation factor of the first vibration mode occurs. This indicates a better collaboration between the frames and a good diaphragm effect. In general, as shown in Fig. 4b, d, f, h, the trend associated with natural frequency for increasing values of k_{r-r} is characterised by three branches: an almost constant trend for both low and high stiffness values, and an almost linear branch for intermediate values. The limits of the pseudo-linear transition phase depend on the uniformity of stiffness among frames (k_{p-p}) and on the effectiveness of the roof-to-beam connections.

4 Non-linear dynamic analysis

A set of non-linear dynamic analyses has been performed to investigate the structural response of the building under seismic action, considering three different types of roof-to-roof connections (none, MSD, and rigid), three types of roof-to-beam connections (angle, dowel, and rigid) and three types of panel-to-panel connections (none, FBD and rigid), for a total of $3 \times 3 \times 3 = 27$ analyses.

The non-linear behaviour of both columns and selected connections is taken into account into the numerical model. Each column is reinforced considering a geometric reinforcement ratio $\rho = 1\%$, with 12 Φ20 mm steel bars made of steel grade B450C ($f_{yk} = 450$ MPa) placed as shown in Fig. 8, with a concrete cover of 30 mm. The steel bars and the concrete core are considered effectively confined by closed stirrups. Sargin model (Sargin and Handa 1969) is used for unconfined concrete. For the confined core, this model is properly modified after peak with a stress plateau up to the ultimate strain evaluated according to the Model Code 2010 (Fib 2010) in order to take into account the confining effects of the

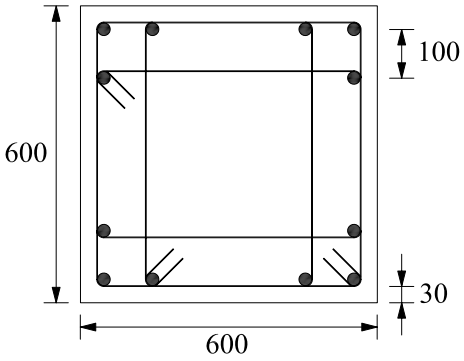

Fig. 8 Column cross-section (dimensions in mm)

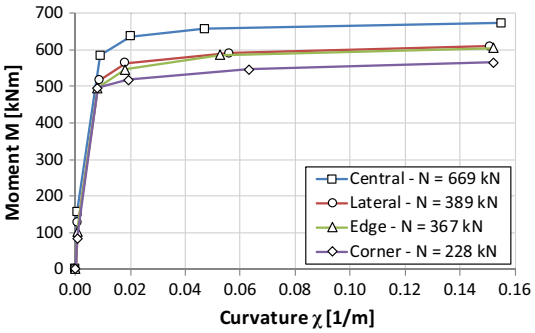

Fig. 9 Non-linear moment–curvature diagrams of columns

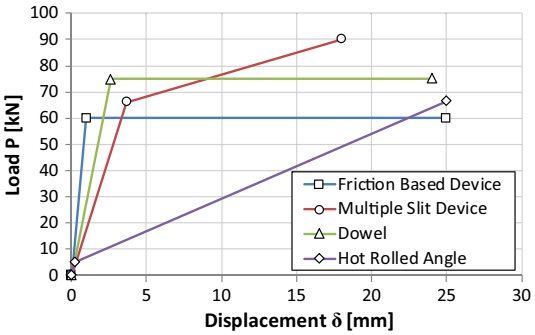

Fig. 10 Non-linear load–displacement diagrams of connections

transversal reinforcement. A linear-parabolic stress–strain relationship is assumed for the steel reinforcement. A smeared plasticity model based on the cross-sectional non-linear moment–curvature relationship is used for the beam elements based on a Takeda hysteretic behaviour considering an unloading stiffness parameter equal to 0.4 (Takeda et al. 1970). The non-linear moment–curvature diagrams of the column cross-section are determined on the base of geometry, mechanical properties and acting axial load in seismic combination (Fig. 9).

The monotonic load–displacement relationships of the connections (FBDs, MSDs, dowels and angles) are shown in Fig. 10. These load–displacement diagrams are calibrated based on the test results collected in Dal Lago et al. (2017a, 2018b), Psycharis and Mouzakis (2012b) and Dal Lago et al. (2017c), respectively. An elastic-plateau monotonic curve is used for both FBDs and dowels. An elastic-hardening monotonic stress–strain relationship is used for both MSDs and angles. A classic kinematic hardening hysteretic behaviour is assumed for FBDs and MSDs. A Takeda hysteretic behaviour is assumed for dowels and angles considering an unloading stiffness parameter equal to 0.4 (Takeda et al. 1970).

The analyses have been performed under the accelerogram shown in Fig. 11. This accelerogram is achieved by analytically enriching in frequency the original signal recorded in Tolmezzo (Italy) during the 1976 earthquake to make it compatible with the elastic response spectrum of Eurocode 8 for soil type B (EN 1998-1:2004). The accelerogram has been scaled to a peak ground acceleration PGA = 0.32 g. This PGA value has been selected to make the results comparable with the ones obtained in a previous numerical

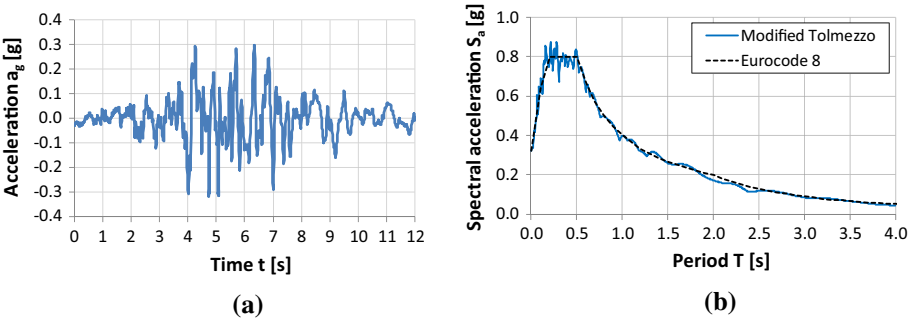

Fig. 11 Modified Tolmezzo accelerogram: **a** accelerogram (PGA = 0.32 g); **b** elastic response spectrum compared with the model of Eurocode 8 for soil type B

investigation performed on a similar precast building, in which the diaphragm has been considered as perfectly rigid (Biondini et al. 2013a).

Table 1 resumes the main seismic performance indicators of the structure for all cases studied. The structure without panel-to-panel connections is characterised by uniform distributions of mass and stiffness among the frames and flexible behaviour with maximum displacements of about 190 mm and similar actions on the columns. Relative displacements between internal and external frames are small also in the configuration without roof-to-roof connections. The effectiveness of the diaphragm increases if angle connections are replaced by stiffer connections.

If rigid or dissipative panel-to-panel connections are placed and there are no roof-to-roof connections, the structural drift can be reduced by means of rigid roof-to-beam connections. The structural drift can be significantly reduced by adding floor-to-floor MSDs, whose effectiveness is reduced if used in combination with angle roof-to-beam connections.

The base shear of the external frame, including also the contribution transmitted by the cladding panels through foundations, is much higher if panel-to-panel connections are considered. However, it is limited by the shear threshold when dissipative panel-to-panel connections are used.

Table 2 provides the main seismic performance indicators of the connections. If panel-to-panel connections are not used, all the combinations of connections lead to limited actions and good diaphragm behaviour. Elsewise, the diaphragm connections are considerably stressed. In particular, without roof-to-roof connections and with dowels between roof and beam, the actions in the dowels lead to yielding and involve sliding of some centimetres of the roof elements, which can cause problems of displacement compatibility.

The introduction of roof-to-roof connections significantly improves the diaphragm effect, reducing the relative displacements with respect to the previous case to about 30%. MSDs activate within the plastic range when angle of dowel roof-to-beam connections are used, thresholding the stress pattern of the deck. The loads increase up to three times if rigid floor-to-floor connections (e.g. welded) are used.

It is worth noting that replacing rigid connections with FBDs allows a reduction of the acting load to 40%. Dissipative connections activate in all cases considered. Angle roof-to-beam connections also activate in all cases.

Figure 12 shows the top displacement time histories of the building without panel-to-panel connections. Central and external frames have different responses in case of flexible

Table 1 Summary of results of the non-linear dynamic analyses: frame system

Connections			Columns			Frames	
Roof-to-roof	Roof-to-beam	Panel-to-panel	Max absolute displacement (mm)	Displacement ratio $\delta_{int,max}/\delta_{ext,max}$ (–)	Max moment (kNm)	Base shear—internal frame (kN)	Base shear—external frame (kNm)
None	Angle	Rigid	215	1497.1	605[a]	232	752
None	Angle	FBD	214	38.4	607[a]	241	1139
None	Angle	None	219	1.4	642[a]	227	232
None	Dowel	Rigid	138	603.6	568	227	1156
None	Dowel	FBD	141	18.2	578	238	1126
None	Dowel	None	195	1.1	620[a]	227	234
None	Rigid	Rigid	138	601.3	567	228	1155
None	Rigid	FBD	39	2.1	283	146	1126
None	Rigid	None	184	1.0	607[a]	222	251
MSD	Angle	Rigid	79	275.5	404	184	1374
MSD	Angle	FBD	84	6.9	409	149	1104
MSD	Angle	None	186	1.0	610[a]	220	247
MSD	Dowel	Rigid	37	114.9	278	144	1516
MSD	Dowel	FBD	36	2.4	263	158	1091
MSD	Dowel	None	184	1.0	611[a]	218	249
MSD	Rigid	Rigid	18	41.6	215	166	2199
MSD	Rigid	FBD	28	1.4	246	136	1144
MSD	Rigid	None	184	1.0	608[a]	225	243
Rigid	Angle	Rigid	16	50.3	189	99	1584
Rigid	Angle	FBD	31	2.1	559	374	1185
Rigid	Angle	None	184	1.0	608[a]	222	245
Rigid	Dowel	Rigid	7	18.3	123	85	1808
Rigid	Dowel	FBD	19	1.1	212	117	1121
Rigid	Dowel	None	184	1.0	608[a]	224	245

Table 1 (continued)

Connections			Columns			Frames	
Roof-to-roof	Roof-to-beam	Panel-to-panel	Max absolute displacement (mm)	Displacement ratio $\delta_{int,max}/\delta_{ext,max}$ (–)	Max moment (kNm)	Base shear—internal frame (kN)	Base shear—external frame (kNm)
Rigid	Rigid	Rigid	5	9.6	90	69	2152
Rigid	Rigid	FBD	16	1.1	188	106	1140
Rigid	Rigid	None	184	1.0	607[a]	224	245

[a]Yielding

Table 2 Summary of results of the non-linear dynamic analyses: connections

Connections			Panel-to-panel connections		Roof-to-beam connections		Roof-to-roof connections	
Roof-to-roof	Roof-to-beam	Panel-to-panel	Max load (kN)	Max relative displacement (mm)	Max load (kN)	Max relative displacement (mm)	Max load (kN)	Max relative displacement (mm)
None	Angle	Rigid	44	0.0	29[a]	10.4	0.0	36.7
None	Angle	FBD	60[a]	1.8	29[a]	10.5	0.0	36.4
None	Angle	None	0	63.1	18[a]	5.5	0.0	14.2
None	Dowel	Rigid	73	0.0	75[b]	5.6	0.0	22.6
None	Dowel	FBD	60[a]	2.5	75[b]	5.8	0.0	21.3
None	Dowel	None	0	58.9	27	0.9	0.0	4.7
None	Rigid	Rigid	73	0.0	464	0.0	0.0	22.7
None	Rigid	FBD	60[a]	6.1	378	0.0	0.0	9.8
None	Rigid	None	0	61.1	80	0.0	0.0	5.0
MSD	Angle	Rigid	86	0.0	23[a]	7.7	82.6[b]	13.6
MSD	Angle	FBD	60[a]	4.0	23[a]	8.0	81.9[b]	13.1
MSD	Angle	None	0	60.7	17[a]	5.2	12.1	0.7
MSD	Dowel	Rigid	96	0.0	46	1.6	69.8[b]	6.0
MSD	Dowel	FBD	60[a]	4.9	41	1.4	70.1[b]	6.2
MSD	Dowel	None	0	60.9	34	1.2	8.0	0.4
MSD	Rigid	Rigid	146	0.0	334	0.0	46.1	2.7
MSD	Rigid	FBD	60[a]	6.5	246	0.0	31.1	1.8
MSD	Rigid	None	0	61.0	102	0.0	7.5	0.4
Rigid	Angle	Rigid	102	0.0	32[a]	11.5	160.9	0.0
Rigid	Angle	FBD	60[a]	4.8	23[a]	7.7	163.8	0.0
Rigid	Angle	None	0	61.1	17[a]	5.1	149.6	0.0
Rigid	Dowel	Rigid	119	0.0	32	1.1	191.3	0.0
Rigid	Dowel	FBD	60[a]	5.7	32	1.1	158.8	0.0
Rigid	Dowel	None	0	61.1	32	1.1	143.5	0.0

Table 2 (continued)

Connections			Panel-to-panel connections		Roof-to-beam connections		Roof-to-roof connections	
Roof-to-roof	Roof-to-beam	Panel-to-panel	Max load (kN)	Max relative displacement (mm)	Max load (kN)	Max relative displacement (mm)	Max load (kN)	Max relative displacement (mm)
Rigid	Rigid	Rigid	141	0.0	108	0.0	219.3	0.0
Rigid	Rigid	FBD	60[a]	4.5	108	0.0	167.9	0.0
Rigid	Rigid	None	0	61.2	108	0.0	130.7	0.0

[a]Activation; [b]Yielding

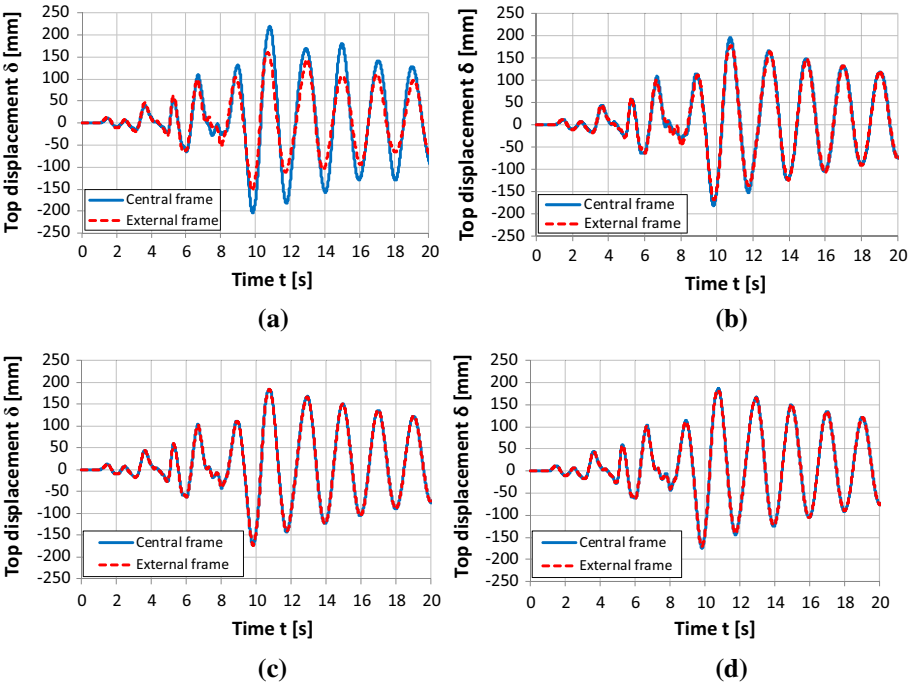

Fig. 12 Top displacement time histories of the building with no panel-to-panel connections: **a** angle roof-to-beam and no roof-to-roof connections; **b** dowel roof-to-beam and no roof-to-roof connections; **c** rigid roof-to-beam and no roof-to-roof connections; **d** angle roof-to-beam and roof-to-roof MSD connections

connections, even if the vibrations are in phase and the differences are limited. It can also be observed that the introduction of MSD roof-to-roof connections leads to a good diaphragm effect also in case of flexible angle roof-to-beam connections.

The base shear versus top displacement diagram, including the contribution of the horizontal action at the base of the cladding panels, is very similar for both cases of effective

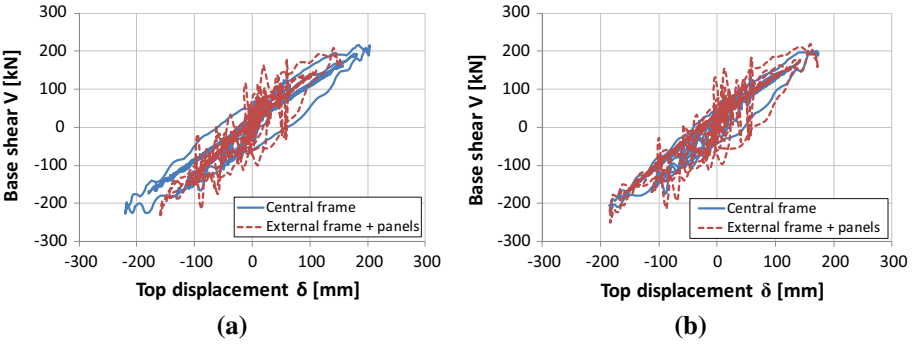

Fig. 13 Base shear versus top displacement hysteretic diagrams of the building with no panel-to-panel and no roof-to-roof connections: **a** angle roof-to-beam connections; **b** rigid roof-to-beam connections

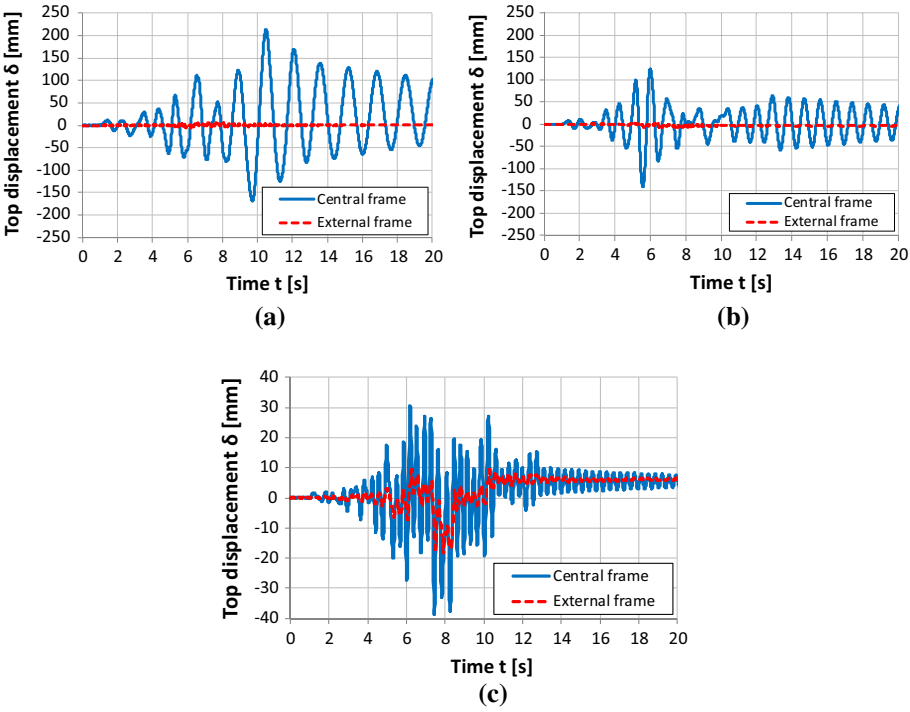

Fig. 14 Top displacement time histories of the building with FBD panel-to-panel and no roof-to-roof connections: **a** angle roof-to-beam connections; **b** dowel roof-to-beam connections; **c** rigid roof-to-beam connections

and deformable diaphragm, as shown in Fig. 13. The base shear of the external frames shows peaks related to the vibration of the stiff panels.

Figure 14 shows the top displacement time histories of the building with FBDs interposed between panels and without roof-to-roof connections. If angle roof-to-beam connections are used, the external frames do not influence the vibration of the central frame (no diaphragm effect). In this configuration, the introduction of dissipative devices between the panels does not avoid the structure to damage.

Dowel connections improve the collaboration among the frames. In this case, the maximum displacement is reduced to about 50%. This allows to avoid yielding at the column bases, even if a significant distortion of the deck occurs.

The top displacement time histories of both external and central frames are in phase and close, even if with non-negligible differences, only when rigid connections are used.

Figure 15 compares the base shear versus top displacement diagrams for the cases of angle and rigid roof-to-beam connections. It is noted that the excellent damping potential of the FBDs is exploited only if rigid deck connections are used. In this case, the relative displacement of the frames is strongly reduced.

As shown in Fig. 16, the use of MSDs in between the roof elements significantly reduces the maximum top displacement of the structure also if angle roof-to-beam connections are used. Moreover, stiffer connections improve more significantly the seismic performance of the overall building.

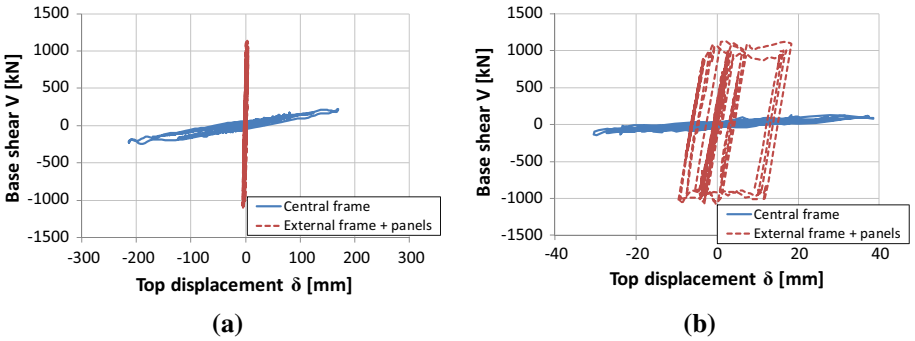

Fig. 15 Shear versus top displacement diagrams of the building with FBD panel-to-panel and no roof-to-roof connections: **a** angle roof-to-beam connections; **b** rigid roof-to-beam connections

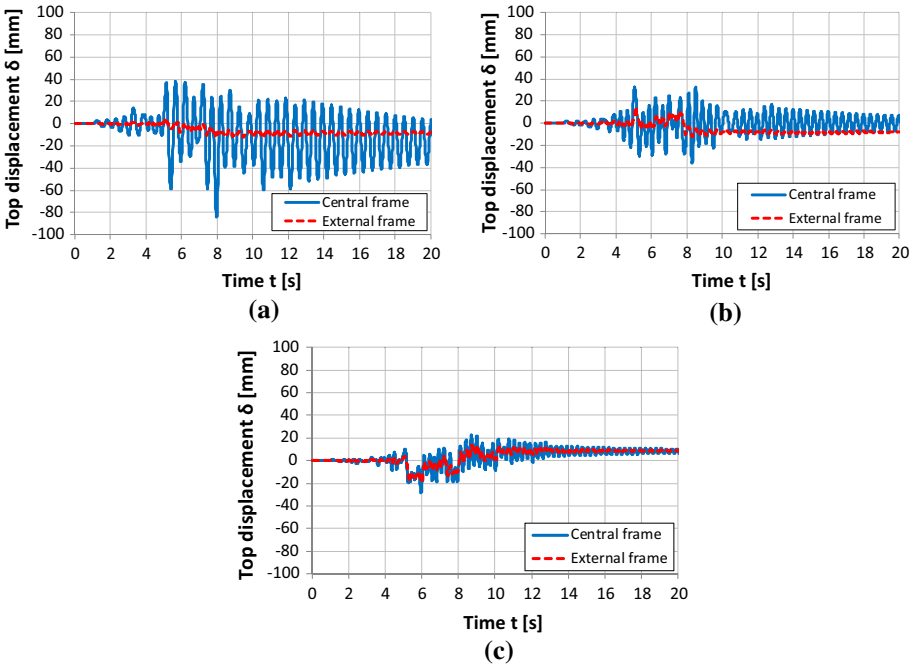

Fig. 16 Top displacement time histories of the building with FBD panel-to-panel and MSD roof-to-roof connections: **a** angle roof-to-beam connections; **b** dowel roof-to-beam connections; **c** rigid roof-to-beam connections

The maximum top displacement attained with MSDs is limited to less than 14 mm for all the studied cases (Table 2). These values are consistent with the characteristics of this kind of device and are associated with the maximum exploitation of its dissipative capacity.

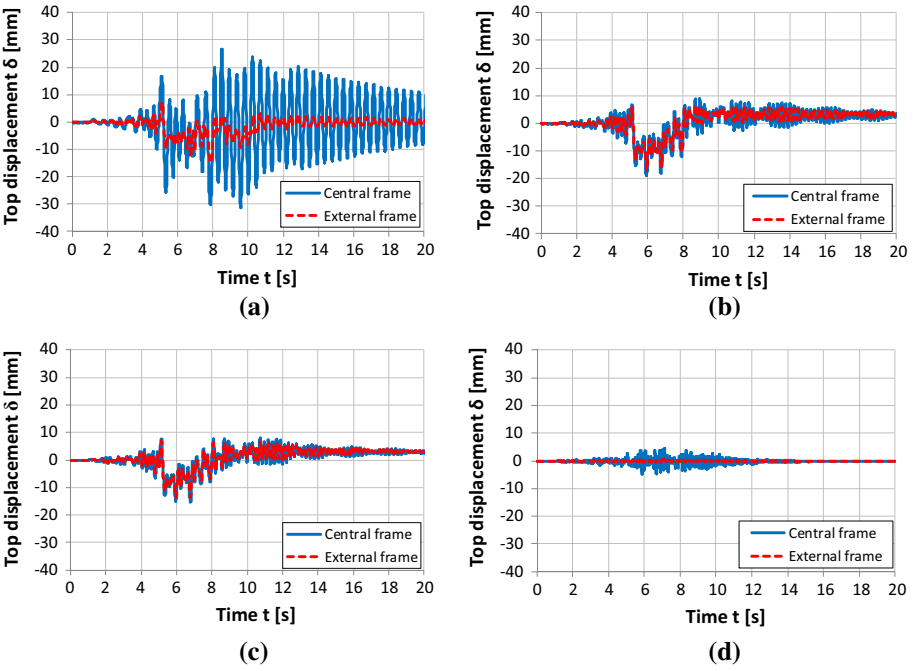

Fig. 17 Top displacement time histories of the building with stiff roof-to-roof connections: **a** FBD panel-to-panel and angle roof-to-beam connections; **b** FBD panel-to-panel and dowel roof-to-beam connections; **c** FBD panel-to-panel and stiff roof-to-beam connections; **d** stiff panel-to-panel and stiff roof-to-beam connections

The maximum displacements of the central frame are further reduced with the use of rigid roof-to-roof connections, such as welds. In this case, as shown in Fig. 17, the diaphragm effect is satisfactory not only if using rigid roof-to-beam connections, but also if using dowels. It is worth noting that welded roof-to-beam connections are difficult to be made and unfrequently used in practice, since they could alter the simply supported static scheme of roof elements under gravity loads by creating a clamped roof-to-beam joint which draws high moments into connections and columns.

5 Conclusions

The problem of the effectiveness of the diaphragm action in single-storey precast concrete frame structures has been investigated. The role of both deck connections (roof-to-roof and roof-to-beam) and cladding panel connections (panel-to-panel) on the seismic response of this type of structures has been investigated by means of both linear and non-linear dynamic analyses.

The results show that both deck and cladding panel connections play a fundamental role on the seismic performance of dry-assembled precast frame structures. Based on these results, the following conclusions can be drawn:

- Uniform distribution of mass and stiffness in precast frame structures can be achieved through the adoption of a statically determined cladding panel connection system;
- Statically undetermined cladding connection systems (dissipative or integrated) lead to relevant differences in terms of stiffness between external and internal frames;
- Uniform distribution of mass and stiffness among the different frames leads to a uniform flexible seismic response of the structure, with both flexible and stiff diaphragm;
- With flexible diaphragm, non-uniform distributions of mass and stiffness cause relevant deck distortion and out-of-phase response of the single frames, without relevant reduction of the seismic drift;
- With stiff diaphragm, non-uniform distributions of mass and stiffness lead to large actions on the elements and connections of both deck and cladding panels;
- Stiff diaphragms may be obtained with stiff roof-to-beam connections, or with flexible roof-to-beam and stiff roof-to-roof connections;
- The forces in the connections can be limited with dissipative cladding connection systems without jeopardising the substantial improvement of the seismic performance of the structure, with relevant limitation of the drift;
- The efficiency of dissipative cladding connection systems is reduced in structures with flexible diaphragm.

Furthermore, the use of low cost dissipative devices between the cladding panels and between the roof elements can remarkably improve the seismic performance of the structure with relevant reduction of drift under forces that are limited by the yield or slip threshold of the devices. The use of MSDs in the deck as floor-to-floor dissipative connections allows to fully exploit the benefits of the installation of panel-to-panel FBDs, protecting the roof elements from excessive rise of forces. This technological solution may allow precast frame structures to be fully operating even after the occurrence of earthquakes with seismic intensity associated with the ultimate limit state design.

The results presented in this paper have been obtained considering a single accelerogram and a given panel aspect ratio. Further studies are necessary to investigate the influence of the panel geometry and the role of uncertainties associated with both the seismic action and structural response by means of a probabilistic analysis.

Acknowledgements The work presented in this paper has been carried out with the financial support of the Italian Department of Civil Protection (DPC) and the Italian Laboratories University Network of Earthquake Engineering (ReLUIS) within the research program DPC-ReLUIS 2014–2016.

References

Babič A, Dolšek M (2016) Seismic fragility functions of industrial precast building classes. Eng Struct 118:357–370

Belleri A (2017) Displacement based design for precast concrete frames with not-emulative connections. Eng Struct 141:228–240

Belleri A, Torquati M, Riva P (2014) Seismic performance of ductile connections between precast beams and roof elements. Mag Conc Res 66(11):553–562

Belleri A, Brunesi E, Nascimbene R, Pagani M, Riva P (2015a) Seismic performance of precast industrial facilities following major earthquakes in the Italian Territory. J Perform Constr Facil 29(5):04014135

Belleri A, Torquati M, Riva P, Nascimbene R (2015b) Vulnerability assessment and retrofit solutions of precast industrial structures. Earthq Struct 8(3):801–820
Belleri A, Torquati M, Marini A, Riva P (2016) Horizontal cladding panels: in-plane seismic performance in precast concrete buildings. Bull Earthq Eng 14(4):1103–1129
Belleri A, Marini A, Riva P, Nascimbene R (2017) Dissipating and re-centring devices for portal-frame precast structures. Eng Struct 150:736–745
Belleri A, Cornali F, Passoni C, Marini A, Riva P (2018) Evaluation of out-of-plane seismic performance of column-to-column precast concrete cladding panels in one-storey industrial buildings. Earthq Eng Struct Dyn 47(2):397–417
Belletti B, Gasperi A, Spagnoli A (2015) Capacity design-based seismic forces in floor-to-beam connections of precast concrete frames. ASCE J Perform Constr Facil 29(6):04014161
Biondini F, Toniolo G (2009) Probabilistic calibration and experimental validation of the seismic design criteria for one-storey concrete frames. J Earthq Eng 13:426–462
Biondini F, Toniolo G, Tsionis G (2010) Capacity design and seismic performance of multi-storey precast structures. Eur J Environ Civil Eng 14(1):11–28
Biondini F, Titi A, Toniolo G (2012) Pseudodynamic tests and numerical simulations on a full-scale prototype of a multi-storey precast structure. In: 15th world conference on earthquake engineering (15WCEE), Lisbon, Portugal, September 24–28, 2012, Paper No. 1468
Biondini F, Dal Lago B, Toniolo G (2013a) Role of wall panel connections on the seismic performance of precast structures. Bull Earthq Eng 11(4):1061–1081
Biondini F, Dal Lago B, Toniolo G (2013b) Diaphragm action in precast structures with cladding wall panels. In: 15th Italian congress on earthquake engineering (ANIDIS 2013), June 30–July 4, 2013, Padua
Bournas DA, Negro P, Molina FJ (2013a) Pseudodynamic tests on a full-scale 3-storey precast concrete building: behaviour of the mechanical connections and floor diaphragms. Eng Struct 57:609–627
Bournas D, Negro P, Taucer F (2013b) Performance of industrial buildings during the Emilia earthquakes in Northern Italy and recommendations for their strengthening. Bull Earthq Eng 12(5):2383–2404
Brunesi E, Nascimbene R, Bolognini D, Bellotti D (2015) Experimental investigation of the cyclic response of reinforced precast concrete frames structures. PCI J 2:57–79
Buratti N, Minghini F, Ongaretto E, Savoia M, Tullini N (2017) Empirical seismic fragility for the precast RC industrial buildings damaged by the 2012 Emilia (Italy) earthquakes. Earthq Eng Struct Dyn 46(4):2317–2335
Casotto C, Silva V, Crowley H, Nascimbene R, Pinho R (2015) Seismic fragility of Italian RC precast industrial structures. Eng Struct 94:122–136
Dal Lago B, Ferrara L (2016) Efficiency of mechanical floor connections on the diaphragm action of precast concrete floor/roof decks. In: 14th international symposium on structural engineering, vol 1, Beijing, pp 469–476
Dal Lago B, Lamperti Tornaghi M (2018) Sliding channel cladding connections for precast structures subjected to earthquake action. Bull Earthq Eng. https://doi.org/10.1007/s10518-018-0410-0
Dal Lago B, Molina FJ (2018) Assessment of a capacity spectrum design approach against cyclic and seismic experiments on full-scale precast RC structures. Earthq Eng Struct Dyn 47(7):1591–1609
Dal Lago B, Toniolo G, Lamperti Tornaghi M (2016) Influence of different mechanical column-foundation connection devices on the seismic behaviour of precast structures. Bull Earthq Eng 14(12):3485–3508
Dal Lago B, Biondini F, Toniolo G (2017a) Friction-based dissipative devices for precast concrete panels. Eng Struct 147:356–371
Dal Lago B, Biondini F, Toniolo G, Lamperti Tornaghi M (2017b) Experimental investigation on the influence of silicone sealant on the seismic behaviour of precast façades. Bull Earthq Eng 15(4):1771–1787
Dal Lago B, Muhaxheri M, Ferrara L (2017c) Numerical and experimental analysis of an innovative lightweight precast concrete wall. Eng Struct 137:204–222
Dal Lago B, Toniolo G, Felicetti R, Lamperti Tornaghi M (2017d) End support connection of precast roof elements by bolted steel angles. Struct Concr 18(5):755–767
Dal Lago B, Biondini F, Toniolo G (2018a) Experimental investigation on steel W-shaped folded plate dissipative connectors for precast cladding panels. J Earthq Eng 22(5):778–800
Dal Lago B, Biondini F, Toniolo G (2018b) Experimental tests on multiple-slit devices for precast concrete panels. Eng Struct 167:420–430
Dal Lago B, Biondini F, Toniolo G (2018c) Seismic performance of precast concrete structures with energy dissipating cladding panel connection systems. Struct Concr. https://doi.org/10.1002/suco.201700233 **(invited paper)**
Dal Lago B, Negro P, Dal Lago A (2018d) Seismic design and performance of dry-assembled precast structures with adaptable joints. Soil Dyn Earthq Eng 106:182–195

Dei Poli S, di Prisco M, Gambarova PG (1992) Shear response, deformations, and subgrade stiffness of a dowel bar embedded in concrete. ACI Struct J 89(6):665–675
Demartino C, Vanzi I, Monti G, Sulpizio C (2017) Precast industrial buildings in Southern Europe: loss of support at frictional beam-to-column connections under seismic actions. Bull Earthq Eng 16(1):259–294
EN 1998-1:2004 (2004) Eurocode 8: design of structures for earthquake resistance. Part 1: General rules, seismic actions and rules for buildings. European Committee for Standardization, Brussels, Belgium
Ercolino M, Bellotti D, Magliulo G, Nascimbene R (2018) Vulnerability analysis of industrial RC precast buildings designed according to modern seismic codes. Eng Struct 158:67–78
Ferrara L, Toniolo G (2008) Design approach for diaphragm action of roof decks in precast concrete buildings under earthquake. In: Walraven J, Stoelhorst D (eds) *fib* Symposium "Taylor made concrete structures", Amsterdam, pp 963–968
Fib (2010) Model code for concrete structures. Fédération Internationale du Béton/International Federation for Structural Concrete, Lausanne
Fischinger M, Kramar M, Isakovic T (2008) Cyclic response of slender RC columns typical of precast industrial buildings. Bull Earthq Eng 6:519–534
Fleischman RB, Farrow KT (2001) Dynamic response of perimeter lateral-system structures with flexible diaphragms. Earthq Eng Struct Dyn 30(5):745–763
Fleischman RB, Farrow KT (2003) Seismic design recommendations for precast concrete diaphragms in long floor span constructions. PCI J 11–12:46–62
Fleischman RB, Naito C, Restrepo J, Sause R, Ghosh SK (2005a) Seismic design methodology for precast concrete diaphragms, part 1: design framework. PCI J 50(5):68–83
Fleischman RB, Naito C, Restrepo J, Sause R, Ghosh SK, Wan G, Schoettler M, Cao L (2005b) Seismic design methodology for precast concrete diaphragms, part 2: research program. PCI J 50(6):14–31
G + D Computing (2010) Using Strand7 (Straus7)—Introduction to the Strand7 finite element analysis system, Ed. 3, Strand7 Pty Limited
Kramar M, Isakovic T, Fischinger M (2010) Seismic collapse risk of precast industrial buildings with strong connections. Earthq Eng Struct Dyn 39:847–868
Magliulo G, Ercolino M, Manfredi G (2014a) Influence of cladding panels on the first period of one-story precast buildings. Bull Earthq Eng 13(5):1531–1555
Magliulo G, Ercolino M, Petrone C, Coppola O, Manfredi G (2014b) Emilia earthquake: the seismic performance of precast RC buildings. Earthq Spectra 30(2):891–912
Magliulo G, Ercolino M, Cimmino M, Capozzi V, Manfredi G (2015) Cyclic shear test on a dowel beam-to-column connection of precast buildings. Earthq Struct 9(3):541–562
Magliulo G, Cimmino M, Ercolino M, Manfredi G (2017) Cyclic shear tests on RC precast beam-to-column connections retrofitted with a three-hinged steel device. Bull Earthq Eng 15(9):3797–3817
Metelli G, Beschi C, Riva P (2011a) Cyclic behaviour of a column-to-foundation joint for concrete precast structures. Eur J Env Civ Eng 15(9):1297–1318
Metelli G, Bettini N, Plizzari G (2011b) Experimental and numerical studies on the behaviour of concrete sandwich panels. Eur J Env Civ Eng 15(10):1465–1481
Muciaccia G, Di Nunzio G, Consiglio A (2017) Behaviour of mono-stud plates in cracked concrete under shear loading. In: 3rd international symposium on connections between steel and concrete (ConSC 2017), September 27–29, Stuttgart
Negro P, Lamperti Tornaghi M (2017) Seismic response of precast structures with vertical cladding panels: the SAFECLADDING experimental campaign. Eng Struct 132:205–228
Negro P, Bournas DA, Molina FJ (2013) Pseudodynamic tests on a full-scale 3-storey precast concrete building: global response. Eng Struct 57:594–608
Orlando M, Piscitelli LR (2018) Experimental investigation on static and cyclic behaviour of flanged unions for precast reinforced concrete columns. Eur J Env Civ Eng 22(8):927–945
Palanci M, Senel SM, Kalkan A (2017) Assessment of one story existing precast industrial buildings in Turkey based on fragility curves. Bull Earthq Eng 15(1):271–289
Pollini AV, Buratti N, Mazzotti C (2018) Experimental and numerical behaviour of dissipative devices based on carbon-wrapped steel tubes for the retrofitting of existing precast RC structures. Earthq Eng Struct Dyn 47(5):1270–1290
Priestley MJN, Sritharan S, Conley JR, Pampanin S (1999) Preliminary results and conclusions from the PRESSS five-story precast concrete test building. Spec Rep PCI J 44(6):42–67
Psycharis IN, Mouzakis HP (2012a) Assessment of the seismic design of precast frames with pinned connections from shaking table tests. Bull Earthq Eng 10(6):1795–1817
Psycharis IN, Mouzakis HP (2012b) Shear resistance of pinned connections of precast members to monotonic and cyclic loading. Eng Struct 41:413–427

Psycharis IN, Kalyviotis IM, Mouzakis HP (2018) Experimental investigation of the response of precast concrete cladding panels with integrated connections under monotonic and cyclic loading. Eng Struct 159:75–88

Saisi A, Toniolo G (1999) Precast RC columns under cyclic loading: an experimental programme oriented to EC8. Stud Res Polit Milano 19:373–414

Sargin M, Handa VK (1969) A general formulation for the stress-strain properties of concrete. Solid Mech Div 3:1–27

Savoia M, Buratti N, Vincenzi L (2017) Damages and collapses in industrial precast buildings after the 2012 Emilia earthquake. Eng Struct 137:162–180

Schoettler MJ, Belleri A, Zhang D, Restrepo JI, Fleischman RB (2009) Preliminary results of the shake-table testing for the development of a diaphragm seismic design methodology. PCI J 54(1):100–124

Schultz AE, Tadros MK, Huo XM, Magaña RA (1994) Seismic resistance of vertical joints in precast shear walls. In: 12th FIP Congress, Fédération Internationale de la Précontrainte (International Federation for Prestressing), May 29–June 2, 1994, Washington, DC

Scotta R, De Stefani L, Vitaliani R (2015) Passive control of precast building response using cladding panels as dissipative shear walls. Bull Earthq Eng 13:3527–3552

Sorace S, Terenzi G (2017) Existing prefab R/C buildings: seismic assessment and supplemental damping-based retrofit. Soil Dyn Earthq Eng 94:193–203

Takeda T, Sozen MA, Nielsen NN (1970) Reinforced concrete response to simulated earthquakes. ASCE J Struct Div 96(12):2557–2573

Titi A, Biondini F (2014) Probabilistic seismic assessment of multistory precast concrete frames exposed to corrosion. Bull Earthq Eng 12(6):2665–2681

Titi A, Biondini F, Toniolo G (2018) Seismic assessment of existing precast structures with dry-friction beam-to-column joints. Bull Earthq Eng 16(5):2067–2086

Toniolo G, Colombo A (2012) Precast concrete structures: the lesson learnt from L'Aquila earthquake. Struct Conc 13(2):73–83

Toniolo G, Dal Lago B (2017) Conceptual design and full-scale experimentation of cladding panel connection systems of precast buildings. Earthq Eng Struct Dyn 46(14):2565–2586

Tsoukantas SG, Tassios TP (1989) Shear resistance of connections between reinforced concrete linear precast elements. ACI Struct J 86(3):242–249

Tullini N, Minghini F (2016) Grouted sleeve connections used in precast reinforced concrete construction—experimental investigation of a column-to-column joint. Eng Struct 127:784–803

Valente M (2013) Improving the seismic performance of precast buildings using dissipative devices. In: 2nd ICRMCE, vol 54, pp 795–804

Vintzeleou EN, Tassios TP (1987) Behavior of dowels under cyclic deformations. ACI Struct J 84(1):18–30

Yuksel E, Karadoğan F, Bal E, Ilki A, Bal A, Inci P (2015) Seismic behavior of two exterior beam-column connections made of normal-strength concrete developed for precast construction. Eng Struct 99:157–172

Yuksel E, Karadoğan F, Ozkaynak H, Khajehdei A, Güllü A, Smyrou E, Bal IE (2017) Behaviour of steel cushions subjected to combined actions. Bull Earthq Eng 16(2):707–729

Zoubek B, Fischinger M, Isakovic T (2015) Estimation of the cyclic capacity of beam-to-column dowel connections in precast industrial buildings. Bull Earthq Eng 13(7):2145–2168

Zoubek B, Fischinger M, Isaković T (2016) Cyclic response of hammer-head strap cladding-to-structure connections used in RC precast buildings. Eng Struct 119:135–148

Zoubek B, Fischinger M, Isaković T (2018) Seismic response of short restrainers used to protect cladding panels in RC precast buildings. J Vib Control 24(4):645–658